# Disorder effects on luminescence in $\delta$-doped $n$-$i$-$p$-$i$ superlattices

C. Metzner, K. Schrüfer, U. Wieser, M. Luber, M. Kneissl, and G.H. Döhler
*Institut für Technische Physik I, Universität Erlangen, Erwin-Rommel-Strasse 1, Erlangen, Germany*
(Received 19 July 1994)

In heavily $\delta$-doped semiconductor superlattices, the quantizing local space charge potential $V(z, \mathbf{r})$ varies with the position $\mathbf{r}$ parallel to the layers, due to the statistical two-dimensional (2D) configuration of dopants. Assuming linear screening, the probability distribution of this fluctuating potential profile is analyzed using a Monte Carlo technique. As a first approximation of the resulting electronic structure, the 1D quantum problem corresponding to each sampled $z$ profile is solved independently, assuming constant electron and hole quasi-Fermi levels throughout the sample. The subband energy fluctuations, the local wave functions, and the resulting luminescence spectra are calculated for different models. The simulated lateral fluctuations of the band edges are strongly non-Gaussian in the vicinity of the doping layers, leading to an exponential low-energy tail in the luminescence. The recombination of carriers populating tail states is drastically suppressed due to increased confinement in the model, which includes the local perturbation of the wave functions. The theoretical results are compared with electroluminescence spectra of a $\delta$-doped GaAs $n$-$i$-$p$-$i$ superlattice. Both the expected non-Gaussian tail and the wave-function shrinkage of the tail states are confirmed by the experiments. Quantitative agreement is achieved without using fitting parameters.

## I. INTRODUCTION

The band tails, which are the origin of the experimentally observed broadening of the luminescence spectra of doped semiconductors, can be described by the semiclassical Kane model[1] as a first approximation. Using linear screening, the probability distribution of the fluctuating potential created by the random configuration of impurities is calculated and the density of states (DOS) of the pure crystal is assumed to be shifted rigidly at each point according to the local value of this fluctuating potential. The average DOS is then obtained by a convolution of the unperturbed DOS with the potential probability distribution. No further distortion of the local DOS or the electronic wave functions is taken into account in this model. The corresponding broadening of the luminescence spectra is also traced back to the local shifts of the one-particle energy spectra in the conduction (CB) and valence bands (VB).

Unger has pointed out[2] that the local potential is not the quantity directly relevant for the luminescence line shape. He introduced effective band edges, the spatial variation of which is smoother than that of the band edges, as an elementary quantum correction to the semiclassical picture. He used this smoothened potential to calculate the statistical broadening of the luminescence spectra.

A more systematic way to include quantum effects is provided by diagrammatic methods in the framework of multiple-scattering theory. Serre and Ghazali[3] applied Klauder's fifth approximation to calculate the broadened DOS and the disturbed electronic Green's function in a doped semiconductor. However, the necessity to perform a configuration average over different impurity arrangements forces drastic approximations in this method. The complex influence of the random potential is replaced by an energy and wave-vector-dependent, but homogeneous effective medium. Thus the spatial fluctuations of the doping density, which are responsible for the deep tails of the broadened DOS, are not accounted for. In principle, it is possible to include them in a self-consistent way,[4] but this method is extremely computer-time consuming for realistic cases.

Over a long period, the study of luminescence in $n$-$i$-$p$-$i$-doped superlattices was focused on the experimental verification of the predicted blueshift of the spontaneous recombination spectrum with increasing excitation, which is due to a corresponding variation of the effective band gap.[5] This demonstrated the specific tunability of the mobile carrier concentration in these systems.

An attempt to gain a detailed theoretical understanding of the luminescence line shape in systems with doped layers of finite thickness has been made[6] using the Hartree approximation for the electronic states, neglecting potential fluctuations completely. The comparison with experiment showed that the fluctuations were strong enough to obscure the multisubband structure of the spectra.

The first step towards a realistic description of the luminescence line shape has been the application of a semiclassical Kane-like method to the quasi-two-dimensional electronic structure of doped superlattices.[7] Although no quantum effects of the fluctuations have been included, a surprisingly good overall agreement with experiments has been found. However, the Gaussian potential fluctuations assumed in this paper could not reproduce the exponential form of the measured low-energy luminescence tail. Additionally, significant deviations of its decay rate were observed, which have been traced back to the enhanced confinement of deep tail states.

The analysis of experimental luminescence spectra and

 

their simulation in the past has been complicated considerably by using doped superlattices with finite $n$- and $p$-doped layer thickness. In these systems the quantization of energy levels has been too small compared to the fluctuation width induced by the random impurity arrangement and thus many subbands had to be considered simultaneously. Actually, the situation was rather similar to a doped bulk semiconductor with properties that depend periodically on the $z$ coordinate on a mesoscopic length scale.

In order to realize the situation of a two-dimensional (2D) system, which is disturbed by an additional random potential, the energy difference $\Delta\epsilon_{10}$ between the ground state and first excited subband should be large compared to the fluctuation width. At the same time, the electron density should be sufficiently high to keep the typical fluctuation below the $\Delta\epsilon_{10}$ limit and to justify the linear screening approximation.

These conditions can be fulfilled best in heavily $\delta$-doped superlattices. Beyond that, the simple geometry of $\delta$-doped $n$-$i$-$p$-$i$ structures is favorable from a theoretical point of view.

In this paper, we study doping-induced disorder effects on the electronic states and on the luminescence spectra of a $\delta$-doped $n$-$i$-$p$-$i$ superlattice with only one relevant electron and heavy hole subband. We use a simulation method which includes quantum effects in a transparent way and uses a realistic statistics for the potential fluctuations. The details of the theory are given in Sec. III. The results are compared to electroluminescence measurements in Sec. IV. In Sec. II we briefly outline the experimental procedure.

## II. EXPERIMENT

Our experimental investigations of the luminescence are based on the electrical tunability of $n$-$i$-$p$-$i$-doped superlattices.[8] This can be achieved by applying selective contacts for the lateral injection of electrons and holes into the $n$ and $p$ layers, respectively, by an external bias voltage. The separation between the quasi-Fermi levels corresponds to the external potential $eU_{np}$ applied between the selective contacts, $\Phi_n - \Phi_p \approx eU_{np}$, if the gradient of $\Phi_n$ and $\Phi_p$ parallel to the layers is small enough to be neglected. This fact is especially useful for a comparison with theoretical calculations. When a forward bias is applied to these contacts, the injected electrons and holes, though spatially separated, can recombine radiatively by tunneling through the potential barrier resulting in electroluminescence (EL) whose upper half maximum energy is expected at

$$\hbar\omega_{1/2} = \Phi_n - \Phi_p \approx eU_{np}. \quad (1)$$

Compared with photoluminescence, electroluminescence experiments have several important advantages. For example, the quasi–Fermi levels $\Phi_n$ and $\Phi_p$ are independent from the growth direction $z$. Thus the emitted photon spectrum is nearly constant for each layer and there is no contribution to the luminescence from the substrate. Beyond that, information about the fraction of radiative recombinations can be obtained by correlating the emitted optical power $P_{\rm opt}$ to the injection current $I_{pn}$.

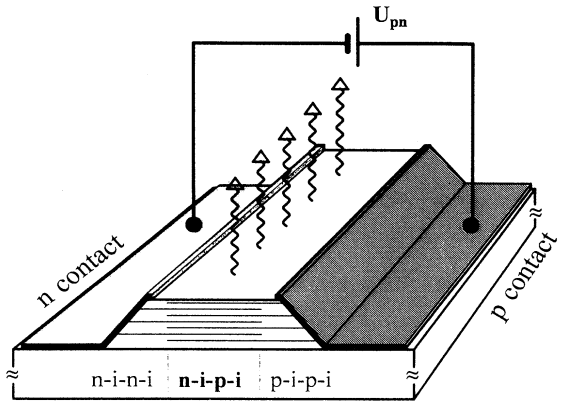


FIG. 1. Schematic of the $\delta$-$n$-$i$-$p$-$i$ device used for EL measurements. The $\delta n$-$i$-$\delta n$-$i$ and the $\delta p$-$i$-$\delta p$-$i$ regions, which result from the shadow growth, form the built-in selective contacts for the $\delta n$ and $\delta p$ layers.

In the past, it has been difficult to apply high-quality contacts selectively to the $n$- and $p$-type layers of the sample. Recently, it has become possible to achieve excellent selective contacts to molecular-beam epitaxial (MBE) grown $n$-$i$-$p$-$i$ structures by a shadow mask

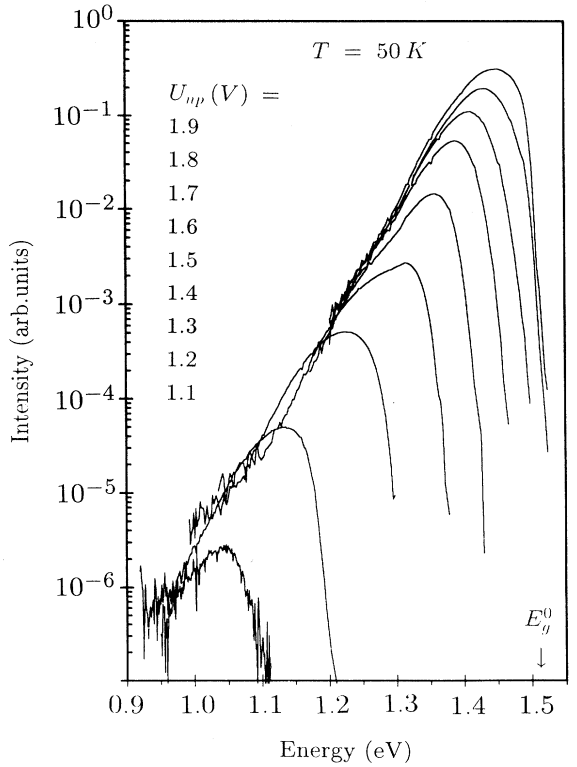


FIG. 2. Measured EL spectra for the GaAs $\delta$-$n$-$i$-$p$-$i$ sample at $T = 50$ K. The corresponding applied bias voltage is shown alongside the spectra.

regrowth technique.[10] Our sample consists of 20 periods of alternating $\delta n$, $i$, $\delta p$, and $i$ layers. The nominal design parameters are $N_D^{(2)} = 6 \times 10^{12}$ cm$^{-2}$ and $N_A^{(2)} = 8 \times 10^{12}$ cm$^{-2}$ for the two-dimensional doping concentrations. The thickness of the undoped $i$ layers was $d_i = 14$ nm. Highly selective, interdigital, lateral $n$ and $p$ contacts were built in during the MBE growth through the shadow mask. Ohmic metal contacts were applied to the $\delta n$-$i$-$\delta n$-$i$ and $\delta p$-$i$-$\delta p$-$i$ regions using standard photolithography. Figure 1 shows schematically the $n$-$i$-$p$-$i$ device structure for our EL measurements.

In Fig. 2 we report the EL spectra of a GaAs $\delta$-$n$-$i$-$p$-$i$-doped superlattice for a set of applied bias voltages as indicated. The spectra were obtained with a typical setup, using a liquid-nitrogen-cooled germanium detector, because of the strongly redshifted luminescence of the $n$-$i$-$p$-$i$ structure at low applied voltage. The spectra were corrected to the response of the optical system. Obviously, the observed EL spectra compare at least qualitatively with the behavior expected from Eq. (1). At a high applied voltage and, therefore, high current, the series resistance lateral to the layers becomes significant, resulting in a reduced blueshift.

For a later detailed comparison with theory we want to point out the low-energy exponential decay of all spectra and the excitation-independent decay constant.

## III. THEORY

### A. The concept

We start with the average state of the system obtained by distributing the donor and acceptor charge homogeneously within the respective doping layers, thus neglecting any statistical potential fluctuations (2D jellium model). Solving the Hartree equations for this case at finite sheet electron and hole densities $\overline{n}^{(2)}$ and $\overline{p}^{(2)}$ yields a self-consistent 1D potential profile $\overline{U}(z)$ and the mean $z$-dependent charge density distributions $\overline{n}^{(3)}(z)$ and $\overline{p}^{(3)}(z)$ of electrons and holes.[9]

The homogeneous doping charge considered above is only the average part of the real distribution, which is a random array of point charges within each layer. The second, remaining part contains — by definition — the doping density fluctuations. Its influence on the mean electron distribution of the jellium system is now analyzed in a second step.

Starting with the mean mobile charge density $\overline{n}^{(3)}(z)$ and $\overline{p}^{(3)}(z)$, the screening properties of the real system can be determined. Using the linear screening approximation we calculate the effective perturbing potential $\Delta U(z, \mathbf{r})$ produced by the fluctuating part of the doping density. By definition, the lateral average $\langle \Delta U(z, \mathbf{r}) \rangle_{\mathbf{r}}$ is zero for all values of $z$. This irregular perturbation of the electron gas breaks the translational invariance of the jellium system parallel to the layers.

In principle, only a genuine 3D quantum theory can solve our problem in a completely satisfactory way. However, if the lateral variation of $\Delta U(z, \mathbf{r})$ is considered to be smooth compared to the mean profile $\overline{U}(z)$ in growth direction, it appears natural to solve the quantum problem corresponding to the total potential $U(z, \mathbf{r}) = \overline{U}(z) + \Delta U(z, \mathbf{r})$ locally and independently at each lateral position $\mathbf{r}$, assuming again translational invariance in each case.

In reality, of course, the supposition of smoothness is violated in the immediate vicinity of each impurity. On the other hand, the extreme numerical effort connected with models accounting also for lateral confinement effects may justify the local approximation studied in this paper.

If the local 1D Schrödinger equations for electrons and holes are solved and the optical transition rates are calculated (assuming constant quasi-Fermi levels throughout the sample), the subband edges, occupation densities, $z$ wave functions, and luminescence spectra are obtained as functions of the position $\mathbf{r}$ parallel to the layers. Afterwards their probability distributions or macroscopic averages can be calculated. In practice, the sampling of different positions $\mathbf{r}$ is replaced by an averaging over different impurity configurations $\tilde{c}$ at the fixed position $\mathbf{r} = \mathbf{0}$.

To give a preliminary impression of the main physical effects covered by our approximation, Fig. 3 schematically shows three examples of the local band structure and corresponding luminescence for a compensated system ($N_D = N_A$) at $T = 0$ K. For the sake of clarity in this figure we disregard the influence of the random acceptor distribution. Also, only one electron and hole subband is considered.

Position $\mathbf{r}_0$ corresponds to the mean configuration $[U(z, \mathbf{r}_0) = \overline{U}(z)]$, as described by the jellium model. In our compensated model system the 2D mobile carrier densities are equal in this case $[n^{(2)}(\mathbf{r}_0) = p^{(2)}(\mathbf{r}_0)]$. Because of the identical Fermi wave vectors of electrons and holes, the high-energy flank of the boxlike luminescence spectrum coincides with the difference $\Delta\Phi_{np}$ between the quasi-Fermi levels.

Position $\mathbf{r}_1$ lies in a zone of enhanced donor concentration, a donor cluster. The attractive potential of the excess donors is reflected in a local reduction of the potential $[U(z, \mathbf{r}_1) < \overline{U}(z)]$ in the $n$-layer region, whereas the potential remains unaltered at the $p$ layer by definition. Therefore the local classical band gap $E_{cv}(\mathbf{r}_1)$ is lower than in the mean case ($\overline{E}_{cv}$).

As the local value $\epsilon_0^{\mathrm{el}}(\mathbf{r}_1)$ of the subband edge refers to the minimum of the potential well $U(z = 0, \mathbf{r}_1)$, which has been shifted towards the band gap, the same shift follows in zeroth order for $\epsilon_0^{\mathrm{el}}(\mathbf{r}_1)$ on an absolute energy scale. Consequently, the local occupation density $n^{(2)}(\mathbf{r}_1)$ of the electron subband increases and thus $n^{(2)}(\mathbf{r}_1) > p^{(2)}(\mathbf{r}_1)$.

At the same time the steeper increase of $U(z, \mathbf{r}_1)$ causes a narrowing of the potential well in $z$ direction, which enhances the quantization effect on the electronic states. As a first result, the eigenvalue $\epsilon_0^{\mathrm{el}}(\mathbf{r}_1)$ increases, partly compensating the reduction of the bottom of the well, so that the effective shift of the subband edge is smaller than that of the conduction band edge.

As a second consequence of the enhanced confinement, the electron wave function becomes more localized in $z$

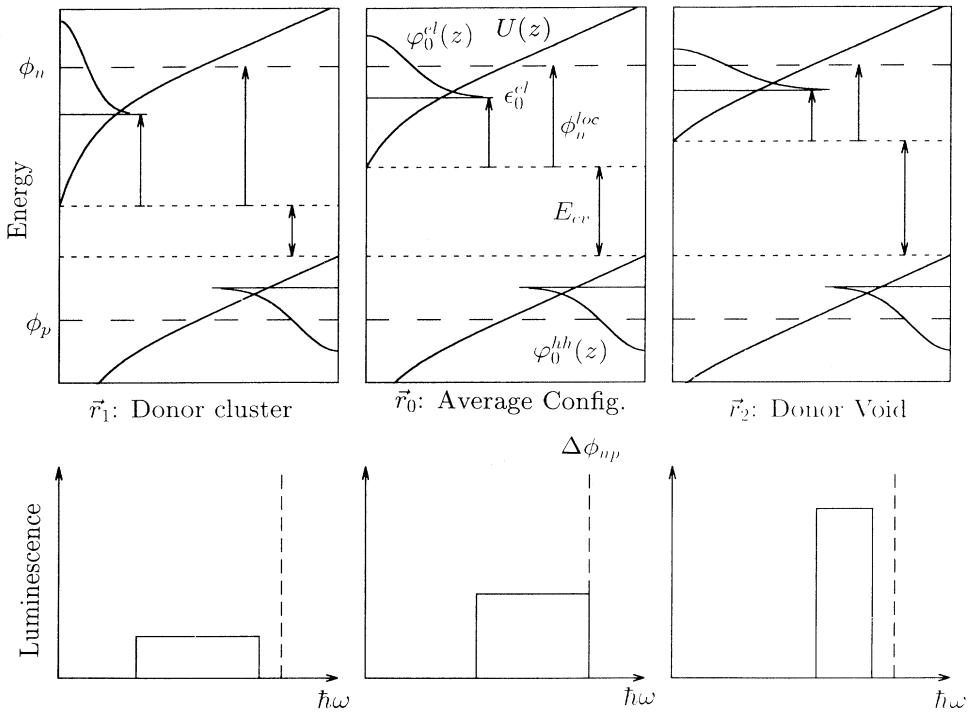


FIG. 3. Local band edge profiles, corresponding quantum states, and luminescence for different positions $\mathbf{r}$ parallel to the layers. Position $\mathbf{r}_0$ refers to the average case (jellium model), $\mathbf{r}_1$ to a donor cluster, and $\mathbf{r}_2$ to a void of donors. The local excitation level of the conduction band is defined as $\phi_n^{\mathrm{loc}} = \phi_n - U(z=0,\mathbf{r})$.

direction and the electron-hole overlap is decreased.

The smallest photon energy that can be emitted is $\hbar\omega_{\min}(\mathbf{r}_1) = E_{cv}(\mathbf{r}_1) + \epsilon_0^{\mathrm{el}}(\mathbf{r}_1) + \epsilon_0^{\mathrm{hh}}$. As the reduction of the first term overcompensates the increase of the second, the low-energy edge of the luminescence spectrum is redshifted (compared to the nominal case $\mathbf{r}_0$). The high-energy edge is now slightly below $\Delta\Phi_{np}$, because of $n^{(2)}(\mathbf{r}_1) \neq p^{(2)}(\mathbf{r}_1)$. This follows directly from $\mathbf{k}$ conservation being assumed for all calculations of luminescence spectra in this paper. Additionally the intensity is diminished due to the overlap effect. In conclusion, the luminescence from donor clusters is weak and redshifted.

Position $\mathbf{r}_2$ corresponds to a void of donors. There, of course, all aspects behave contrary to the cluster case. Especially, the lack of donors reflects in a rise of the bottom of the $n$ layer and in a widening of the well shape, which weakens the quantization. Again, quantum mechanics results in an attenuation of the fluctuations (the rise of the subband edge is smaller than that of the conduction band edge). The $z$ wave function is slightly less localized. The luminescence from donor voids is more intensive and blueshifted.

It is easy to visualize that averaging over random donor and acceptor distributions yields luminescence spectra with tails extending to lower energies than in the jellium model. However, as strongly redshifted recombination processes exhibit reduced transition probabilities, one expects tails in the luminescence spectra that decay significantly faster than in a model without locally varying wave functions.

In the following we will provide a more detailed and sound theoretical formulation of the ideas outlined in this section. In particular we will present different models of increasing degree of sophistication.

### B. Local equations

Assume the local configuration of impurities $\tilde{c}$ is given by the positions $\mathbf{r}_{n,i}$ and $\mathbf{r}_{p,j}$ of donors and acceptors in the $n$ and $p$ layers. For simplicity, we use the same microscopic donor arrangement for all $n$ layers (and analogously for the $p$ layers), thus conserving the $2d_i$ periodicity in $z$ direction. This leads to a well defined parity of the quantum states discussed later on. As a further consequence, only a half period of the system (the region between an $n$ layer at $z=0$ and the neighboring $p$ layer at $z=d_i$) has to be considered. The screened potential fluctuations in this region are almost totally due to the two adjacent doping layers, because of the small screening lengths.

Within a linear screening model, the resulting local perturbation of the band edge $z$ profile is

$$\Delta U(z,\tilde{c}) = \sum_{i\in\tilde{c}} \Delta U^0_{\mathrm{don}}(z,\mathbf{r}_{n,i}) + \sum_{j\in\tilde{c}} \Delta U^0_{\mathrm{acc}}(z-d_i,\mathbf{r}_{p,j})\,, \tag{2}$$

where $\Delta U^0(z-z_0,\mathbf{r}_0)$ denotes the screened potential of a single impurity located at position $\mathbf{R}_0 = (z_0,\mathbf{r}_0)$. Consequently, the effective quantizing potential acting on the electron/hole gas is

$$U(z,\tilde{c}) = \overline{U}(z) + \Delta U(z,\tilde{c})\,. \tag{3}$$

By definition, we set $\overline{U}(z=0)=0$.

In the case of electrons (el), we have to solve the Schrödinger equation

$$\left[-\frac{\hbar^2}{2m^*_{\rm el}}\frac{\partial^2}{\partial z^2}+[U(z,\tilde{c})-\Delta U(z=0,\tilde{c})]\right]\varphi^{\rm el}_\mu(z,\tilde{c}) = \epsilon^{\rm el}_\mu(\tilde{c})\varphi^{\rm el}_\mu(z,\tilde{c})\,. \quad (4)$$

The constant term $-\Delta U(z=0,\tilde{c})$ assures that the eigenvalue $\epsilon^{\rm el}_\mu(\tilde{c})$ of the $\mu$th electron subband refers to the bottom of the conduction band quantum well (compare Fig. 3). Therefore, on an absolute energy scale, the subband edge is at

$$E^{\rm el}_\mu(\tilde{c})=\Delta U(z=0,\tilde{c})+\epsilon^{\rm el}_\mu(\tilde{c})\,. \quad (5)$$

Analogous equations hold for the heavy (hh) and light (lh) holes.

Due to the assumption of lateral translation invariance, the total local wave function reads

$$\Psi^{\rm el}_{\mu\mathbf{k}}(\mathbf{R},\tilde{c})=\Omega^{-1/2}\varphi^{\rm el}_\mu(z,\tilde{c})\,e^{i\mathbf{k}\cdot\mathbf{r}} \quad (6)$$

and the local dispersion relation reads

$$E^{\rm el}_\mu(\mathbf{k},\tilde{c})=\Delta U(z=0,\tilde{c})+\epsilon^{\rm el}_\mu(\tilde{c})+\alpha_{\rm el}\,k^2\,, \quad (7)$$

with $\alpha_{\rm el}=\hbar^2/2m^*_{\rm el}$. Note that in our local model the plane wave part $e^{i\mathbf{k}\cdot\mathbf{r}}$ of the total wave function extends only over a finite region of the $x$ and $y$ directions.

The luminescence intensity as a function of photon energy is given by

$$I(\hbar\omega,\tilde{c})\propto\frac{1}{\omega}\sum_{h=\rm lh,hh}|P_{\rm el,h}|^2\sum_{\mu\nu}\,|\,\langle{\rm el},\mu,\tilde{c}\,|\,h,\nu,\tilde{c}\rangle_z\,|^2 \times Z_{\mu\nu}(\hbar\omega,\Phi_n,\Phi_p,T,\tilde{c})\,, \quad (8)$$

where $P_{{\rm el},h}$ is the matrix element of the momentum operator in the bulk system,

$$\langle{\rm el},\mu,\tilde{c}\,|\,h,\nu,\tilde{c}\rangle_z=\int dz\,\varphi^{\rm el}_\mu(z,\tilde{c})\,\varphi^h_\nu(z,\tilde{c}) \quad (9)$$

is the local overlap matrix element, and $Z_{\mu\nu}$ the combined optical density of states. Using the Fermi function

$$f(x,T)=\frac{1}{e^{x/k_BT}+1} \quad (10)$$

the latter can be written as

$$Z_{\mu\nu}(\hbar\omega,\Phi_n,\Phi_p,T,\tilde{c})=\frac{\Theta(\Delta E_{\mu\nu}(\hbar\omega))}{4\pi(\alpha_{\rm el}+\alpha_h)}f\left[E^{\rm el}_\mu(\tilde{c})+\left(\frac{\alpha_{\rm el}}{\alpha_{\rm el}+\alpha_h}\right)\Delta E_{\mu\nu}(\hbar\omega,\tilde{c})-\Phi_n,T\right] \times f\left[E^h_\nu(\tilde{c})+\left(\frac{\alpha_h}{\alpha_{\rm el}+\alpha_h}\right)\Delta E_{\mu\nu}(\hbar\omega,\tilde{c})-\Phi_p,T\right]\,, \quad (11)$$

with the kinetic part of the recombination energy

$$\Delta E_{\mu\nu}(\hbar\omega,\tilde{c})=\hbar\omega-[E_{cv}(\tilde{c})+\epsilon^{\rm el}_\mu(\tilde{c})+\epsilon^h_\nu(\tilde{c})]\,. \quad (12)$$

Note that we measure the hole energy $\epsilon^h_\nu(\tilde{c})$ relative to the valence band maximum (bottom of the $p$-layer quantum well) in such a manner that it increases in the direction away from the gap. For the definition of the classical band gap

$$E_{cv}(\tilde{c})=E^0_g-[U(z=d,\tilde{c})-U(z=0,\tilde{c})] \quad (13)$$

see Fig. 3. The quantities $\Phi_n$ and $\Phi_p$ are the quasi-Fermi levels, which are constant throughout the sample.

The above formulas have to be evaluated separately for each of the $N_{\rm conf}$ sampled impurity configurations $\tilde{c}$. Then the macroscopically visible luminescence spectrum is simply given by

$$\overline{I}(\hbar\omega)=\frac{1}{N_{\rm conf}}\sum_{\tilde{c}}I(\hbar\omega,\tilde{c})\,. \quad (14)$$

The probabiliy distribution of an arbitrary locally fluctuating quantity $x(\tilde{c})$ is defined through

$$P(x)=\frac{1}{N_{\rm conf}}\sum_{\tilde{c}}\delta(x-x(\tilde{c}))\,. \quad (15)$$

In this paper we apply this formula to the local subband edges $E^{\rm el}_\mu$, $E^{\rm hh}_0$ and the local band edge extrema $\Delta U(z=0)$, $\Delta U(z=d)$.

As mentioned in Sec. III A, it is necessary to perform a self-consistent Hartree calculation before simulating the fluctuations, in order to obtain the averaged state and screening properties of the system. We denote the corresponding electronic eigenvalues by $\overline{\epsilon}^{\rm el}_\mu$ and the $z$ wave functions by $\overline{\varphi}^{\rm el}_\mu(z)$. Analogous symbols are used for the averaged hole states.

The density profile of the electrons is then given by

$$\overline{n}^{(3)}(z)=\sum_\mu\overline{n}_\mu(\Phi_n,T)\,\left|\overline{\varphi}^{\rm el}_\mu(z)\right|^2\,, \quad (16)$$

with the 2D subband occupation density

$$\overline{n}_\mu(\Phi_n,T)=\int dE\,\frac{m^*_{\rm el}}{\pi\hbar^2}\,\Theta(E-\overline{\epsilon}^{\rm el}_\mu)f(E-\Phi_n,T)\,. \quad (17)$$

### C. Screened impurity potential

Considering the 2D nature of the electron/hole gas (strong quantization) and the inhomogeneous mobile charge distributions $\overline{n}^{(3)}(z)$ and $\overline{p}^{(3)}(z)$, it seems to be essential to use a quantum-mechanical screening approximation like the random-phase approximation (RPA).

However, beyond the fact that the ordinary RPA only yields matrix elements of the screened potential instead of the potential itself, it has been demonstrated[11] that (at least in our standard system) the RPA can be replaced by the semiclassical (and isotropical) Thomas-Fermi theory without significant changes in the results. This is due to the large mobile charge density at the doping layers, which causes screening lengths significantly smaller than the intrinsic layer thickness $d_i$.

The inverse quadratic screening length $L_n^{-2}$ of the electron gas is calculated at the position of the donors, at $z = 0$, according to

$$L_n^{-2} = \left( \frac{3^{1/3} e^2 m_{\mathrm{el}}^*}{\pi^{4/3} \hbar^2 \epsilon_r \epsilon_0} \right) \left[ \overline{n}^{(3)}(z=0) \right]^{1/3} . \tag{18}$$

Similarly, for the hole gas we use

$$L_p^{-2} = \left( \frac{3^{1/3} e^2 m_{\mathrm{hh}}^*}{\pi^{4/3} \hbar^2 \epsilon_r \epsilon_0} \right) \left[ \overline{p}^{(3)}(z=d_i) \right]^{1/3} . \tag{19}$$

Within the isotropic Thomas-Fermi approximation the screened potential of a point charge has the analytical Yukawa form. Therefore a donor at position $(z = 0, \mathbf{r}_{ni})$ produces the following potential $z$ profile along the $\mathbf{r} = \mathbf{0}$ axis:

$$\Delta U^0_{\mathrm{don}}(z, \mathbf{r}_{n,i}) = -\frac{e^2}{4\pi\epsilon_r\epsilon_0} \frac{e^{-\sqrt{z^2+|\mathbf{r}_{ni}|^2}/L_n}}{\sqrt{z^2+|\mathbf{r}_{ni}|^2}} . \tag{20}$$

For an acceptor at position $(z = d_i, \mathbf{r}_{pj})$ we obtain

$$\Delta U^0_{\mathrm{acc}}(z-d_i, \mathbf{r}_{p,j}) = +\frac{e^2}{4\pi\epsilon_r\epsilon_0} \frac{e^{-\sqrt{(z-d_i)^2+|\mathbf{r}_{pj}|^2}/L_p}}{\sqrt{(z-d_i)^2+|\mathbf{r}_{pj}|^2}} . \tag{21}$$

It should be emphasized that these are the effective potentials due to complete impurity point charges. As already discussed in the Introduction, the actual perturbing charge distribution is an array of point charges minus the average part (homogeneously charged plate), which defined the unperturbed system. Thus, if the total random potential $\Delta U(z, \mathbf{r})$ of the whole $n$ and $p$ layer were calculated using the above single impurity potentials, its lateral average would not be zero as required.

### D. Simulation of local potential profile

Due to the short screening lengths in our system, the fluctuating part $\Delta U(z, \mathbf{r} = \mathbf{0})$ of the total potential is dominated by a relatively small number of impurities close to the axis $\mathbf{r} = \mathbf{0}$ (this has been demonstrated in Ref. 11). Therefore the impurity configuration $\tilde{c}$ can be restricted to the $M$ nearest donors and the $N$ nearest acceptors. For the system parameters studied in this paper, the potential probability distributions converge for $M, N > 50$.

As the screening is isotropic parallel to the layers, only the lateral distances $r_{ni}, r_{pj}$ of the impurities from the axis are necessary to calculate their total perturbing $z$ profile:

$$\tilde{c} = \{ r_{ni}, r_{pj} \mid ni, pj \text{ nearest neighbors to } \mathbf{r} = \mathbf{0} \} . \tag{22}$$

If the 2D doping density in the $n$ layer is $N_D$, the probability to find the nearest donor neighbor at distance $r_{n1}$, the second nearest donor at distance $r_{n2}, \ldots$, is

$$P(r_{n1}, r_{n2}, \ldots, r_{nM}) = e^{-N_D \pi r_M^2} \prod_{i=1}^{M} (2\pi N_D r_{ni}) . \tag{23}$$

A random list of increasing distances $r_{ni}$ (corresponding to the $i$th nearest donor neighbor), which satisfies the probability distribution Eq. (23), can be generated using the following recursive algorithm:

$$r_{n0} = 0, \qquad r_{ni} = \sqrt{\left( r_{n,i-1}^2 + \frac{1}{\pi N_D} \right) \ln\left( \frac{1}{1-z_i} \right)} , \tag{24}$$

where the $z_i$ are random numbers equally distributed in the interval $[0, 1[$.

The same can be done for the $N$ acceptor neighbors. Then the resulting local perturbation of the band edge $z$ profile $\Delta U(z, \tilde{c})$ can be calculated using Eq. (2) together with Eq. (20) and Eq. (21).

Repeating the procedure for a sufficiently large number $N_{\mathrm{conf}}$ of configurations $\tilde{c}$, we obtain a statistically independent ensemble of $z$ profiles equivalently to sampling randomly the lateral positions within the layers.

In order to fulfill the zero-mean condition, we first calculate the average $z$ perturbation of the ensemble:

$$\langle \Delta U(z) \rangle_{\tilde{c}} = \frac{1}{N_{\mathrm{conf}}} \sum_{\tilde{c}} \Delta U(z, \tilde{c}) . \tag{25}$$

In a second step we subtract this function from each individual local perturbation:

$$\Delta U'(z, \tilde{c}) = \Delta U(z, \tilde{c}) - \langle \Delta U(z) \rangle_{\tilde{c}} . \tag{26}$$

The new ensemble has the required property:

$$\frac{1}{N_{\mathrm{conf}}} \sum_{\tilde{c}} \Delta U'(z, \tilde{c}) = 0 . \tag{27}$$

### E. The models

If the luminescence spectra are calculated for each local impurity configuration and finally added up, the average spectrum represents the complex result of various, qualitatively different effects such as fluctuations of the wave functions, the energy levels, occupation numbers, and band edges. It is therefore instructive to compare the results with other approximations, in order to isolate the single fluctuation effects as far as possible.

In this paper we study a series of four models, labeled A – D, in which certain quantities are kept fixed at their mean values.

#### 1. Model A

The theory of this model has been described in detail in the preceding part of the paper. It is the most realistic approximation, where all the quantities, which are relevant for the luminescence, are fluctuating.

#### 2. Model B

Here the simulation works exactely as in model A, with the exception that the wave functions $\varphi_\mu^{\rm el}(z,\tilde{c})$ and $\varphi_\nu^h(z,\tilde{c})$ are held constant:

$$\varphi_\mu^{\rm el}(z,\tilde{c}) \to \overline{\varphi}_\mu^{\rm el}(z)\,, \quad \varphi_\nu^h(z,\tilde{c}) \to \overline{\varphi}_\nu^h(z)\,. \tag{28}$$

Therefore the comparison with approximation A gives direct information about the importance of the localization-delocalization effect on the spectral tail.

#### 3. Model C

Here we additionally fix the eigenvalues $\epsilon_\mu^{\rm el}(\tilde{c})$ and $\epsilon_\nu^h(\tilde{c})$:

$$\epsilon_\mu^{\rm el}(\tilde{c}) \to \overline{\epsilon}_\mu^{\rm el}\,, \quad \epsilon_\nu^h(\tilde{c}) \to \overline{\epsilon}_\nu^h\,. \tag{29}$$

This means that we now have a Kane-like, semiclassical model, where the fluctuation of the subband edges follows rigidly that of the band edges. The comparison with model B demonstrates the quantum-mechanical damping effect on the fluctuations. It should be noted, as the band edges are varying relative to the constant quasi-Fermi levels, the occupation densities of the subbands are still functions of the lateral position.

#### 4. Model D

This is the most naive approach to calculate the broadening of the luminescence. It differs from model C by disregarding the readjustments of the carrier densities and Fermi energies. In this model, the quasi-Fermi levels are not constant but fluctuate for different configurations according to

$$\Phi_n \to \Phi_n + \Delta U(z=0,\tilde{c})\,, \quad \Phi_p \to \Phi_p - \Delta U(z=d_i,\tilde{c})\,. \tag{30}$$

Here, the only fluctuating quantity in the expression for the luminescence spectrum is the classical band gap $E_{cv}(\tilde{c})$, which controls the energy onset of the spectrum. As the shape of the boxlike spectrum is unaltered, the average luminescence is simply a convolution of the nominal spectrum with the probability distribution function of $E_{cv}(\tilde{c})$. The comparison with model C demonstrates the influence of mobile charge density fluctuations and the relevance of the concept of spatially constant quasi-Fermi levels.

## IV. RESULTS AND DISCUSSION

### A. The 2D jellium model

We consider two different excitation levels $\Delta\Phi_{np}$ of the experimentally investigated system at the temperature $T = 50$ K. Table I shows for the jellium system (without any fluctuations) the corresponding filling factor $F = \overline{n}^{(2)}/N_D^{(2)}$, the modulation amplitude of the sawtooth-shaped $z$ profile of the band edges $\overline{U}_{\rm mod}$, the classical band gap $\overline{E}_{cv}$, the quasi-Fermi levels $\Phi_n, \Phi_p$, the subband edges $\overline{\epsilon}_\mu^c$, and the screening lengths $L_n$, $L_p$.

TABLE I. Parameters for the jellium model.

| | $\Delta\Phi_{np} = 1170$ meV | $\Delta\Phi_{np} = 1400$ meV |
|---|---|---|
| $F$ | 0.14 | 0.48 |
| $\overline{V}_{\rm mod}$ (meV) | 540 | 384 |
| $\overline{E}_{cv}$ (meV) | 974 | 1130 |
| $\Phi_n$ (meV) | 129 | 189 |
| $\overline{\epsilon}_0^{\rm el}$ (meV) | 98 | 89 |
| $\overline{\epsilon}_1^{\rm el}$ (meV) | 222 | 189 |
| $\Phi_p$ (meV) | 77 | 83 |
| $\overline{\epsilon}_0^{\rm hh}$ (meV) | 60 | 55 |
| $\overline{\epsilon}_0^{\rm lh}$ (meV) | 100 | 86 |
| $L_n$ (nm) | 4.6 | 3.8 |
| $L_p$ (nm) | 1.4 | 1.3 |

For both excitation levels, only the ground state subbands of the electrons and heavy holes are significantly occupied. This situation of course may change if fluctuations are considered.

Analyzing the screening properties we find that the screening lengths are smaller than the intrinsic layer thickness of the sample. Due to the exponential decay of the Yukawa potential, the donor fluctuations have almost no influence on the $p$ layer and vice versa. Thus the local quantum states should be uncorrelated in both layers.

The following theoretical results refer to the lower excitation $\Phi_{np} = 1170$ meV. However, the qualitative features remain valid also for the higher excitation level.

### B. Band edge fluctuations

Figure 4 shows the lateral probability distributions of the fluctuating part $\Delta U(z,\mathbf{r})$ of the potential or band

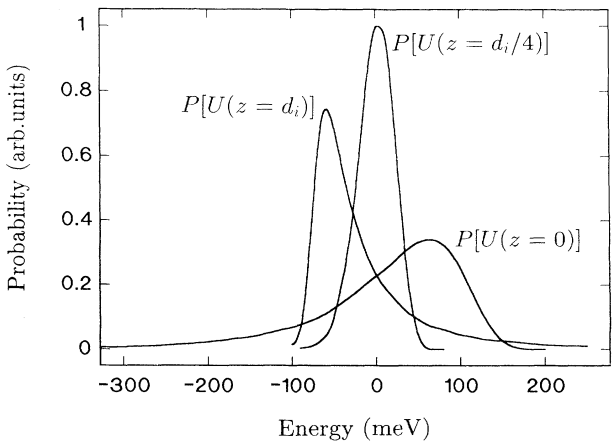


FIG. 4. Probability distributions of the local band edge at different values of $z$.

edge at the doping layers ($z = 0$ and $z = d_i$) and at $z = d_i/4$. The mean value of all these distributions is zero, as required.

A comparison of $P[\Delta U(z = 0, \mathbf{r})]$ with $P[\Delta U(z = d_i/4, \mathbf{r})]$ demonstrates that the width of the band edge fluctuations depends strongly on the distance from the doping layers. This is quantitatively reflected in the standard deviation $\Delta v(z/L_s)$ of the considered probability distributions as a function of $z$, which can be calculated using the Holtsmark method.[7] The contribution of the $n$ layer is given by

$$\Delta v(z/L_n) = \frac{e^2}{\sqrt{8\pi}\epsilon_r\epsilon_0}\sqrt{N_D}\int_1^\infty dx\,\frac{e^{-2(|z|/L_n)x}}{x}\,. \quad (31)$$

The standard deviations obtained in the Monte Carlo simulation agree with the formula above. Obviously the fluctuation width is an exponentially decreasing function of the dimensionless distance $z/L_S$ and diverges logarithmically at the layer position $z = 0$. The width at half maximum, however, remains finite at $z = 0$, because the distribution function takes on a highly asymmetric shape near the layers, with a tail extending far into the band gap. In contrast to that, at $z = d_i/4$ the probability distribution is quasi-Gaussian (suppression of higher statistical moments).

This difference in the shape can be understood considering the number of impurities effectively contributing to the fluctuations. Due to the finite range of the screened impurity potentials, only the nearest neighbors to a given point of the $\mathbf{r} = \mathbf{0}$ axis are relevant, as already discussed.

Within the layer the influence of the first neighbor is much larger than that of the second. If, in the extreme case, the screening length $L_s$ were small compared to the mean interimpurity distance $\bar{r}_{ii}$, we could use the first-nearest-neighbor distribution function, which is known to be extremely asymmetric. It should be noted that the asymmetry is indeed more pronounced for $P[\Delta U(z = d_i, \mathbf{r})]$, because of the small hole screening length.

At sufficiently large distance from the doping layers, the contributions of the $M$ nearest dopants are comparable. If $M$ is large, the central limit theorem predicts a Gaussian probability distribution function, which is adequately characterized by its second moment.

We conclude that the Gaussian or second moment approximation is not sufficient to describe the potential fluctuations in the vicinity of the doping layers.

### C. Fluctuation of energy levels

The distribution functions in Fig. 5 describe the fluctuating conduction band edge $P[U(z = 0)]$, as well as the levels of the electronic ground state $P[\epsilon_0^{\mathrm{el}}]$ and first excited state $P[\epsilon_1^{\mathrm{el}}]$ on an absolute energy scale (the reference point of which is the average conduction band edge). It is remarkable that the mean energy of the subband levels agrees surprisingly well with the value of the jellium model, despite the nonlinear quantization effects involved.

Most important, the width of the level distributions is significantly smaller than that of the band edge, demonstrating directly the quantum-mechanical damping effect on the fluctuations. Especially the low-energy tail, which corresponds to the locally pulled down and narrowed $z$ profiles at impurity clusters, is efficiently reduced by the compensating quantization effect.

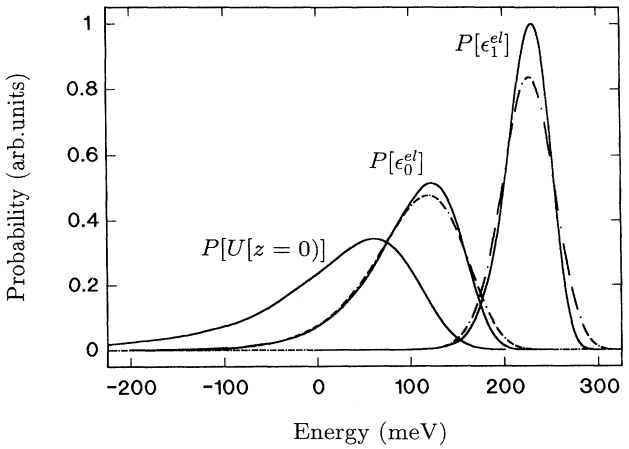


FIG. 5. Probability distributions of the CB minimum $P[U(z = 0)]$, the electronic ground state level $P[\epsilon_0^{\mathrm{el}}]$, and the first excited level $P[\epsilon_1^{\mathrm{el}}]$. The dashed lines correspond to a first order perturbational calculation.

If we look at the statistics of the $\mathrm{el}_1$ level in Fig. 5, the difference in width and shape of the distribution is even more pronounced. In this case $P[\epsilon_1^{\mathrm{el}}]$ can be well approximated by a Gaussian function. The reason is, of course, the reduced density of the $\mathrm{el}_1$ electrons in the region of strong potential fluctuations around the $n$ layer.

In the case of the heavy holes (Fig. 6), the level distribution $P[\epsilon_0^{\mathrm{hh}}]$ is much closer to $P[U(z = d_i)]$. This is due to the large effective mass of these particles. They react nearly like classical particles to the potential fluctuations, i.e., they follow them almost rigidly. Only extremely narrow potential wells can cause a noticeable quantization here.

The energy shift of the electronic subband levels

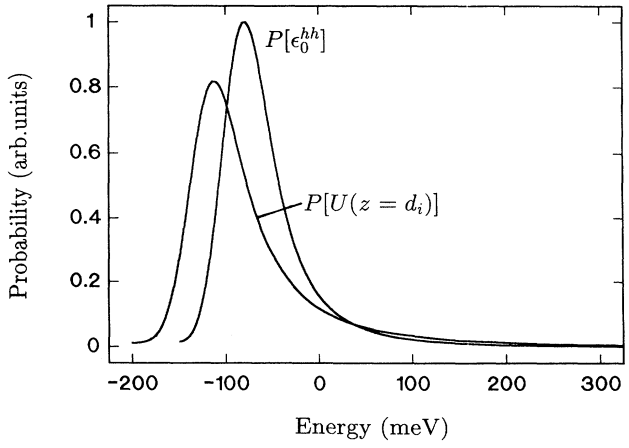


FIG. 6. Probability distributions of the VB maximum $P[U(z = d_i)]$ and the heavy hole ground state level $P[\epsilon_0^{\mathrm{hh}}]$.

$\Delta\epsilon_\mu^{\rm el}(\tilde{c}) = \epsilon_\mu^{\rm el}(\tilde{c}) - \bar{\epsilon}_\mu^{\rm el}$ is given with high accuracy by the quantum-mechanical expectation value

$$\Delta\epsilon_\mu^{\rm el} = \langle \overline{\varphi}_\mu^{\rm el}(z) \mid \Delta U(z,\tilde{c}) \mid \overline{\varphi}_\mu^{\rm el}(z) \rangle \ , \tag{32}$$

which is similar to first order perturbation theory. The corresponding distribution functions are shown as dashed lines in Fig. 5.

We conclude that the inclusion of quantum effects is necessary for a realistic description of the locally fluctuating density of states. The DOS could be easily obtained from the above distributions by convolution with the Heaviside step function.

### D. Luminescence spectrum in the jellium model

To give an impression of the importance of the doping-induced randomness on the luminescence, Fig. 8 includes a comparison of an idealized spectrum, calculated in the jellium model at an excitation level ($\Delta\Phi_{np} = 1170$ meV) neglecting any fluctuations, with the corresponding experimental spectrum, measured at the voltage $U_{np} = 1.2$V. The high-energy wing is well described even in this extremely simplified model, because it merely reflects the thermal energy distribution of electrons and holes above the quasi-Fermi levels, which is not significantly altered by the disorder. However, the measured low-energy tail is completely absent in the jellium system. Here, the luminescence spectrum shows a sharp edge at the photon energy corresponding to the difference between the electron and hole ground state levels.

### E. Luminescence spectra of the disordered system

Figure 7 shows the calculated emission intensity as a function of photon energy for our four simulation models. Obviously the statistical broadening is considerable in each of the studied approximations.

We start with the discussion of the simple semiclassical convolution model D. As the width of the jellium model spectrum $\Delta\hbar\omega_{\rm jel}$ is small compared to the typical $E_{cv}$ fluctuation, the result of the convolution is mainly an energetic shift of the $E_{cv}$ distribution. Especially, the luminescence photon energy exceeds the difference of the quasi-Fermi levels considerably. This is in contrast to the other models, which show a relatively sharp high-energy wing at $\Delta\Phi_{np}$. Beyond that, the exponential low-energy tail decays unrealistically slowly.

A similar decay rate is found in model C, which also neglects any quantum effects completely. The regard of spatially constant quasi-Fermi levels now leads to a physically reasonable high-energy wing, in agreement with the more advanced approximations.

We now turn to the quantum models B and A. The inclusion of the energetic quantization effect in model B seems not to alter the exponential form of the tail, but already leads to a significantly steeper slope compared to the semiclassical approximations. It should be mentioned that in Ref. 11 an excellent agreement has been demonstrated between the B spectrum and a model using the method of first order perturbation theory (mentioned above) and RPA screening.

Finally, the localization-delocalization effect in model A causes an additional, dramatic suppression of the low-energy luminescence tail, while conserving its exponential shape.

In Ref. 7, the luminescence of *n-i-p-i*-doped superlattices has been calculated using Gaussian probability distributions and without accounting for the local wavefunction changes. The resulting spectra showed a non-exponential low-energy tail too, in contrast to the corresponding experimental data. Additionally, the theoretical width of the spectra slightly exceeded the experimental one. Both problems can be solved, in principle, by model A.

### F. Comparison with experiment

In Fig. 8, the theoretical results of models A and B are compared to the corresponding experimental data.

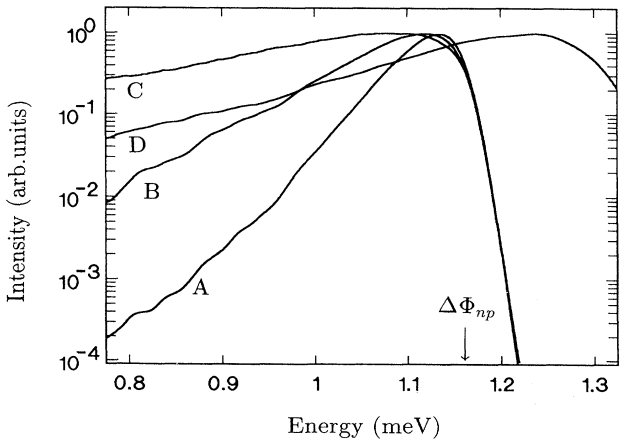


FIG. 7. Luminescence spectra of the disordered system calculated for models A–D at excitation level $\Delta\Phi_{np} = 1170$ meV.

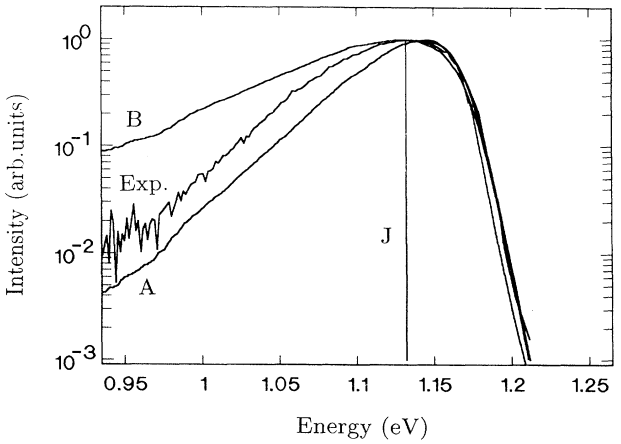


FIG. 8. Luminescence spectra of the jellium system ($J$) and of the disordered system (models A and B) at excitation level $\Delta\Phi_{np} = 1170$ meV, compared to the experimental spectrum at $U_{np} = 1.2$ V.

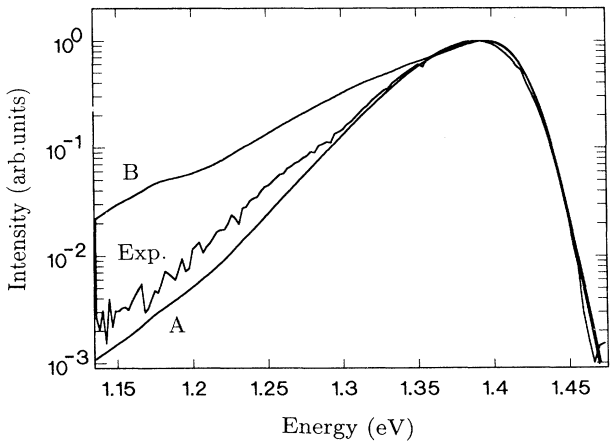


FIG. 9. Luminescence spectra of the disordered system (models A and B) at excitation level $\Delta\Phi_{np} = 1400\,\text{meV}$, compared to the experimental spectrum at $U_{np} = 1.6$ V.

In Fig. 9, the analogous distributions are plotted for the higher excitation level.

Obviously the agreement of the high-energy wing is excellent in both cases. The low-energy tail of the experimental spectra can be well described by an exponential law, with a decay constant that is very close to the simulated value of model A.

The measured spectral widths slightly exceed the simulated ones. On the experimental side, this can be due to an inhomogeneous spatial distribution of the excitation level between the $n$ and $p$ contacts or to a nonuniform doping density of different $n$ and $p$ layers. Theoretical explanations could be the neglect of lateral quantum effects, or the breakdown of the one-band effective mass approximation for states penetrating deeply into the potential wells.

We are not able to observe different subband transitions (such as $\text{el}_0$-$\text{lh}_0$ or $\text{el}_1$-$\text{hh}_0$) in the CB-VB luminescence for higher excitation levels, either in the experiment, or in the theoretical calculations, which can be attributed to the strong potential fluctuations. This stands in contrast to the results published by Schubert *et al.*[12] even for higher doped samples.

The situation is different for CB-intraband transitions between different electron subbands, which can be experimentally investigated, for example, using resonant inelastic Raman scattering. As the edges of the ground and excited electron subbands react on local potential fluctuations in a strongly correlated way, we expect a relatively small statistical broadening of the energy difference $\epsilon_1^{\text{el}} - \epsilon_0^{\text{el}}$. Thus Raman spectroscopy may allow the observation of different subbands even in strongly doped $\delta$-$n$-$i$-$p$-$i$ structures. Details concerning this point will be published soon.[13]

## V. SUMMARY AND CONCLUSION

In this paper we have applied a Monte Carlo method to calculate the probability distribution of the random potential profile in $\delta$-$n$-$i$-$p$-$i$ systems. We have also presented a simple, numerically tractable approximation to include quantum effects on the density of states and luminescence into the theory.

The potential fluctuations are extremely asymmetric near the doping layers and Gaussian-like at the center of the intrinsic layer. The local fluctuations of the wave functions significantly influence the exponential low-energy tail of the luminescence.

A comparison with experimental luminescence spectra shows a good agreement of the line shape over a large range of excitation levels, but deviates significantly from calculations without taking into account the local wavefunction fluctuations. This clearly demonstrates the importance of the quantum effects.

Our simulation method is a flexible tool for the theoretical analysis of disorder effects on the electron gas in doped, quasi-2D semiconductor structures. It could be applied easily to metal-oxide-semiconductor (MOS) systems, doped heterojunctions, or quantum wells.

## ACKNOWLEDGMENTS

We want to thank the Deutsche Forschungsgemeinschaft (DFG, Bonn, Germany) for the financial support. We are very grateful to J.S. Smith, University of California, Berkeley, for the opportunity to grow the sample at his laboratory.

[1] E.O. Kane, Phys. Rev. **131**, 79 (1963).
[2] K. Unger, Ann. Phys. (Leipzig) **27**, 161 (1971).
[3] J. Serre and A. Ghazali, Phys. Rev. B **28**, 4704 (1983).
[4] J. Serre, A. Ghazali, and P. Leroux Hugon, Phys. Rev. B **23**, 1971 (1981).
[5] For a review see K. Ploog and G.H. Döhler, Adv. Phys. **32**, 285 (1983); G.H. Döhler, IEEE J. Quantum Electron. **QE-22**, 1682 (1986).
[6] H.J. Beyer, C. Metzner, J. Heitzer, and G.H. Döhler, Superlatt. Microstruct. **6**, 3 (1989).
[7] M. Renn, C. Metzner, and G.H. Döhler, Phys. Rev. B **48**, 11 220 (1993).
[8] G. Hasnain, G.H. Döhler, J.R. Whinnery, J.N. Miller, and A. Dienes, Appl. Phys. Lett. **49**, 1357 (1986).
[9] K. Schrüfer, S. Eckl, C. Metzner, H.J. Beyer, and G.H. Döhler, J. Appl. Phys. **72**, 4992 (1992).
[10] K.H. Gulden, X. Wu, J.S. Smith, P. Kiesel, A. Höfler, M. Kneissl, P. Riel, and G.H. Döhler, Appl. Phys. Lett. **62**, 1 (1993).
[11] C. Metzner, Ph.D. thesis, University Erlangen–Nürnberg, Germany, 1994.
[12] E.F. Schubert, T.D. Harris, J.E. Cunningham, and W. Jan, Phys. Rev. B **39**, 11 011 (1989).
[13] K. Schrüfer, C. Metzner, and G.H. Döhler, Superlatt. Microstruct. (to be published).